

Multi-Proxy, Multi-Season Streamflow Reconstruction with Mass Balance Adjustment

Hung Nguyen¹, Stefano Galelli¹, Chenxi Xu², and Brendan Buckley³

¹Singapore University of Technology and Design

²Institute of Geology and Geophysics Chinese Academy of Sciences

³Lamont-Doherty Earth Observatory, Columbia University

November 24, 2022

Abstract

Despite having offered important hydroclimatic insights, streamflow reconstructions still see limited use in water resources operations, because annual reconstructions are not suitable for decisions at finer time scales. Attempts towards sub-annual reconstructions have relied on statistical disaggregation, which uses none or little proxy information. Here, we develop a novel framework that optimizes proxy combinations to simultaneously produce seasonal and annual reconstructions. Importantly, the framework ensures that total seasonal flow matches annual flow closely. This mass balance criterion is necessary to avoid misleading water management decisions, such as water allocation. Using the framework, and leveraging a multi-species network of ring width and cellulose $\delta^{18}\text{O}$ in Southeast Asia, we reconstruct seasonal and annual inflow to Thailand's largest reservoir. The reconstructions are statistically skillful. This work is one step closer towards operational usability of streamflow reconstruction in water resources management.

Multi-Proxy, Multi-Season Streamflow Reconstruction with Mass Balance Adjustment

Hung T.T. Nguyen¹, Stefano Galelli¹, Chenxi Xu^{2,3}, and Brendan M. Buckley⁴

¹Pillar of Engineering Systems and Design, Singapore University of Technology and Design, Singapore

²Key Laboratory of Cenozoic Geology and Environment, Institute of Geology and Geophysics, Chinese

Academy of Sciences, Beijing, China

³CAS Center for Excellence in Life and Paleoenvironment, Beijing, China

⁴Lamont-Doherty Earth Observatory, Columbia University, New York, USA

Key Points:

- Ring width and $\delta^{18}\text{O}$ are combined to reconstruct dry season, wet season, and annual streamflow
- Optimal proxy combinations are found with an automatic input selection scheme
- Mass-balance adjustment improves the agreement between seasonal and annual reconstructions

Corresponding author: Hung Nguyen, tanthaihung.nguyen@mymail.sutd.edu.sg

Abstract

15
16 Despite having offered important hydroclimatic insights, streamflow reconstructions still
17 see limited use in water resources operations, because annual reconstructions are not suit-
18 able for decisions at finer time scales. Attempts towards sub-annual reconstructions have
19 relied on statistical disaggregation, which uses none or little proxy information. Here,
20 we develop a novel framework that optimizes proxy combinations to simultaneously pro-
21 duce seasonal and annual reconstructions. Importantly, the framework ensures that to-
22 tal seasonal flow matches annual flow closely. This mass balance criterion is necessary
23 to avoid misleading water management decisions, such as water allocation. Using the
24 framework, and leveraging a multi-species network of ring width and cellulose $\delta^{18}\text{O}$ in
25 Southeast Asia, we reconstruct seasonal and annual inflow to Thailand's largest reser-
26 voir. The reconstructions are statistically skillful. This work is one step closer towards
27 operational usability of streamflow reconstruction in water resources management.

Plain Language Summary

28
29 Long history of river discharge, or streamflow, can be reconstructed from tree rings.
30 These reconstructions help us understand the water cycle in the past, but they have not
31 been widely used in water resources operations. This is because reconstructions are of-
32 ten annual (having only one data point per year). By combining different tree species
33 and different features of tree rings (for example, ring width and stable isotope ratio), it
34 is possible to reconstruct seasonal streamflow in addition to the annual one, and that
35 is our first goal. But a major challenge arises: how do we ensure that the total flow vol-
36 ume of the seasonal reconstructions closely matches the annual one? This criterion is called
37 mass balance, and it is important to avoid misleading water management decisions such
38 as allocating water to different sectors. We develop a novel method to reconstruct sea-
39 sonal and annual streamflow while accounting for mass balance at the same time. Our
40 work is thus a step closer towards operational usability of streamflow reconstructions in
41 water resources management.

1 Introduction

Dendrohydrology, the study of past hydroclimate using tree rings, has been largely motivated by water resources management. The field traces back to Hardman and Reil (1936), who recognized that instrumental records were too short to understand drought trends, and demonstrated that better understanding could be gained from exploring the links between tree rings and streamflow. Their work was motivated by contemporary droughts that affected irrigation. Also to understand droughts, Schulman (1945) established a tree ring chronology for the Colorado River Basin, this time motivated by the war effort—to examine Hoover Dam’s hydropower production reliability to meet wartime demand. While these early works stopped at studying tree ring indices, dendrohydrology took a big step when Stockton (1971), leveraging advanced multivariate techniques (Fritts et al., 1971), showed that reconstructing streamflow record back in time was feasible—long term surface water availability could now be quantified directly. Soon, multiple streamflow reconstructions were developed across the Colorado River Basin (Stockton & Jacoby, 1976), revealing the shortcomings of the Colorado River Compacts (Woodhouse et al., 2006), and providing insights about long term hydrology of Lake Powell, the United States’ second largest reservoir.

Streamflow reconstruction has become “an important planning and research tool” in water resources management (Meko & Woodhouse, 2011). Yet, its use in practical, operational aspects of water management is still limited. That is because reconstructions often target specific components of the hydrograph that best correlated with tree ring proxies. Perhaps most commonly, reconstructions from ring width often target the growth season (e.g., D’Arrigo, Abram, et al., 2011; Güner et al., 2017). Another example is given by reconstructions targeting peak flow using tree ring cellulose stable oxygen isotope ratio ($\delta^{18}\text{O}$) (C. Xu et al., 2019). These reconstructions reveal important insights about the hydroclimate, but do not provide the total annual surface water availability. Other works target the annual flow (e.g., Rao et al., 2018; Nguyen & Galelli, 2018), but even so, the annual resolution is not suitable for making operational decisions at finer time scales—crop planning, for instance, is often based on seasonal flow; reservoir releases are determined at monthly or even weekly time steps.

The water resources community recognizes the need for sub-annual reconstructions. Attempts towards this goal have relied on statistical disaggregation, assuming some statistical relationships between the sub-annual and annual flows (Prairie et al., 2008; Sauchyn & Ilich, 2017). These assumptions are reasonable but not always valid (Figure S1). More importantly, paleoclimatic proxies are not used in these methods, and their rich information are not utilized. Recent progress was made by Stagge et al. (2018), who used multi-species chronologies as additional inputs to disaggregation, showing that these inputs can be weighted differently for each month to improve the monthly reconstructions.

The works of Stagge et al. (2018), C. Xu et al. (2019), and others discussed above suggest that different proxies have different seasonal sensitivities. Therefore, instead of disaggregation, we propose to use multiple proxies to simultaneously reconstruct sub-annual (e.g., seasonal) and annual flows. Two challenges arise. How to combine prox-

ies optimally for different targets? And how to ensure that the seasonal flows add up to the annual flow, i.e., how to account for mass balance? We develop a unified framework to address both challenges. Mass balance is accounted for by a term in the regression formulation that penalizes the differences between total seasonal flow and annual flow (Section 3.1), and proxy combination is optimized with an automatic input selection scheme (Section 3.2). We test the framework with a case study in the Chao Phraya River Basin, Thailand, pooling together a multi-species network of ring width and cellulose $\delta^{18}\text{O}$ chronologies from Southeast Asia (Section 2). This work is one step closer towards operational usability of streamflow reconstruction in water resources management.

2 Study Site and Data

2.1 The Southeast Asian Dendrochronology Network

Over the past three decades, an extensive network of tree ring chronologies have been developed in Southeast Asia. This network has been instrumental in improving our understanding of Southeast Asia’s hydroclimate and history. Tree ring data from Thailand and northern Vietnam (Buckley, Palakit, et al., 2007; Sano et al., 2009) revealed a multidecadal drought, what is later known as the Strange Parallel Droughts (E. R. Cook et al., 2010), which coincided with a tumultuous period of Southeast Asian history (Lieberman, 2003; Lieberman & Buckley, 2012). Further back in time, tree ring data from southern Vietnam linked megadroughts in the 14th and 15th centuries to the demise of the Angkor Civilization (Buckley et al., 2010, 2014). These findings are among many insights that the Southeast Asian Dendrochronology Network has brought forth.

In this work, we use twenty tree ring chronologies from Vietnam, Laos, Cambodia, Thailand, and Myanmar (Figure 1). The chronologies at Kirirom, Petchaburi, Pha Taem, and Wiang Haeng are published here for the first time. The metadata of the chronologies are provided in Table 1. The common period of most chronologies in our network is 1748–2005 (Figure S6), and is the same as the time span of our $\delta^{18}\text{O}$ network. Several chronologies are some decades shorter. Following Stagge et al. (2018), we imputed the missing years using the R package `missMDA` (Josse & Husson, 2016) (see Figure S7). We imputed the tree ring data instead of building nested models because nesting is not applicable in our reconstruction framework. As we shall explain in Section 3.1, the framework is designed to account for mass balance, tuning the regression parameters such that the total sub-annual flow matches the annual flow closely. With nesting, the final variance correction can disrupt the mass balance.

2.2 Cellulose $\delta^{18}\text{O}$

We use four chronologies of tree ring cellulose stable oxygen isotope ratio ($\delta^{18}\text{O}$) that were developed in Laos, Thailand, and Vietnam over the past decade (Figure 1 and Table 2). $\delta^{18}\text{O}$ exhibits strong mechanical and statistical relationship with the hydroclimate (C. Xu et al., 2011; Sano et al., 2012), and has been used to reconstruct wet season precipitation in the region (C. Xu et al., 2015, 2018). $\delta^{18}\text{O}$ in Laos was also found

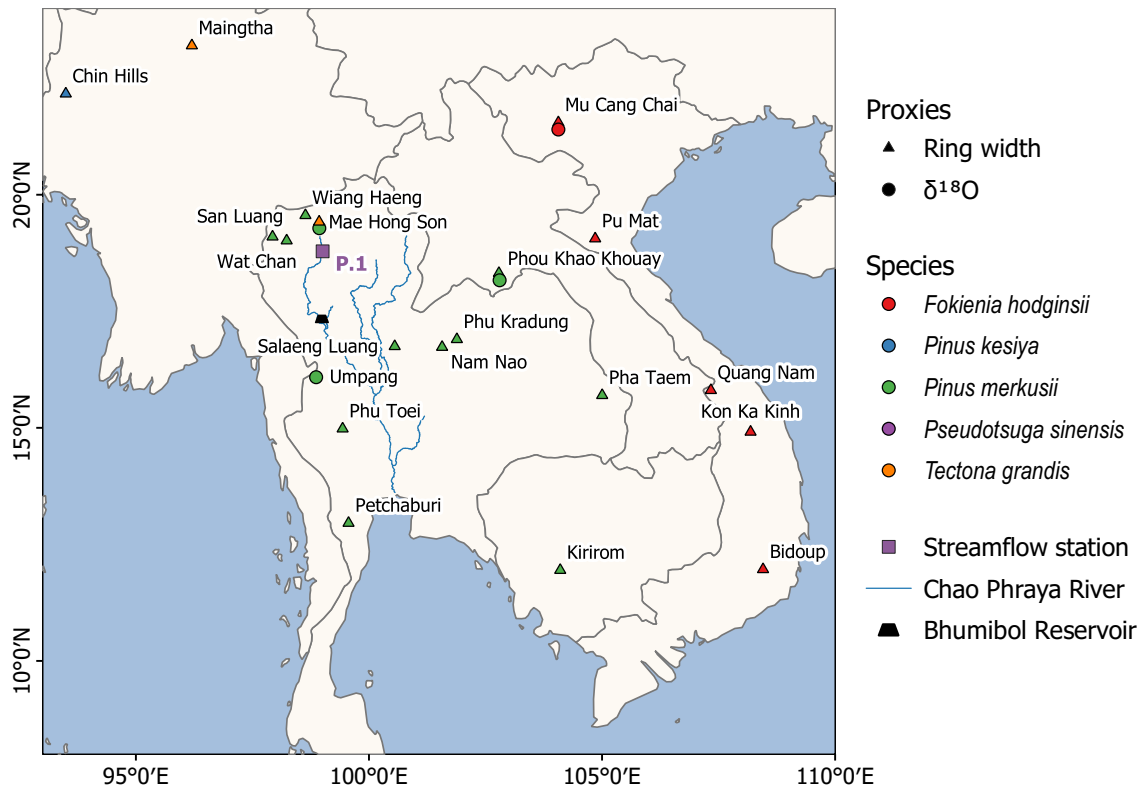


Figure 1. Map of the study region, showing the Chao Phraya River, the proxy network, and the target streamflow station.

123 to have significant negative correlation with Mekong River water level (C. Xu et al., 2013),
 124 suggesting promising hydrological applications. Finally, three $\delta^{18}\text{O}$ chronologies were used
 125 to reconstruct Chao Phraya River peak season flow (C. Xu et al., 2019). These works
 126 support recent literature (Treydte et al., 2006; G. Xu et al., 2019) that $\delta^{18}\text{O}$ has indeed
 127 moved beyond “potential” (Gagen et al., 2011), and earned its place as a practical, valu-
 128 able paleoclimate proxy.

129 2.3 Streamflow

130 The Chao Phraya River Basin covers 30% of Thailand’s area, and is home to about
 131 25 million people. Thailand’s largest reservoir, the Bhumibol (active capacity 9.7 km^3),
 132 lies on the Ping River tributary. Reliable operations of this reservoir require accurate
 133 assessment of inflow availability, on both inter- and intra-annual scales.

134 Streamflow station P.1 is located upstream of Bhumibol Reservoir. P.1 has the longest
 135 and most complete record in Thailand: daily data are available from April 1921–present.
 136 Since 1985, the river upstream of P.1 has been impounded by the Mae Ngat Dam, which,
 137 at full capacity, stores about 14% of P.1’s mean annual flow. Dam operations modify the
 138 seasonal streamflow patterns, thereby interfering with the proxy-streamflow relationship.
 139 Therefore, we naturalized the streamflow data from 1985. The naturalization process is

Table 1. Metadata of tree ring width chronologies.

Site	Longitude	Latitude	Species	References
Bidoup	108.45	11.97	<i>Fokienia hodginsii</i>	Buckley et al. (2010)
Chin Hills	93.50	22.17	<i>Pinus kesiya</i>	Rao (2020)
Kim Hy	106.04	22.25	<i>Pseudotsuga sinensis</i>	Hansen et al. (2017)
Kirirom	104.10	11.95	<i>Pinus merkusii</i>	This study ^a
Kon Ka Kinh	108.18	14.91	<i>Fokienia hodginsii</i>	Buckley et al. (2019)
Mae Hong Son	98.93	19.28	<i>Tectona grandis</i>	Buckley, Palakit, et al. (2007)
Maingtha	96.20	23.20	<i>Tectona grandis</i>	D'Arrigo, Palmer, et al. (2011)
Mu Cang Chai	104.06	21.40	<i>Fokienia hodginsii</i>	Sano et al. (2009)
Nam Nao	101.57	16.73	<i>Pinus merkusii</i>	Buckley et al. (1995)
Petchaburi	99.56	12.96	<i>Pinus merkusii</i>	This study
Pha Taem	105.00	15.70	<i>Pinus merkusii</i>	This study
Phou Khao Khouay	102.79	18.32	<i>Pinus merkusii</i>	Buckley, Duangsathaporn, et al. (2007)
Phu Kradung	101.88	16.90	<i>Pinus merkusii</i>	D'Arrigo et al. (1997)
Phu Toei	99.43	14.98	<i>Pinus merkusii</i>	E. R. Cook et al. (2010)
Pu Mat	104.85	19.06	<i>Fokienia hodginsii</i>	Buckley et al. (2019)
Quang Nam	107.33	15.81	<i>Fokienia hodginsii</i>	Buckley et al. (2017)
Salaeng Luang	100.55	16.75	<i>Pinus merkusii</i>	Buckley et al. (1995)
San Luang	97.93	19.10	<i>Pinus merkusii</i>	E. R. Cook et al. (2010)
Wat Chan	98.23	19.02	<i>Pinus merkusii</i>	Buckley et al. (1995)
Wiang Haeng	98.64	19.56	<i>Pinus merkusii</i>	This study

^a Several cores from this site were analyzed by Zhu et al. (2012) for $\delta^{18}\text{O}$ but the ring width chronology has not been published until now.

Table 2. Metadata of $\delta^{18}\text{O}$ chronologies.

Site	Longitude	Latitude	Species	References
Mae Hong Son	98.93	19.28	<i>Pinus merkusii</i>	C. Xu et al. (2015)
Mu Cang Chai	104.06	21.40	<i>Fokienia hodginsii</i>	Sano et al. (2012)
Phou Khao Khouay	102.79	18.32	<i>Pinus merkusii</i>	C. Xu et al. (2019)
Umpang	98.87	16.09	<i>Pinus merkusii</i>	C. Xu et al. (2018)

140 described in Text S3. After naturalization, we aggregated daily data into dry season (November–
 141 June), wet season (July–October), and water year (November–October). The season de-
 142 lineation was determined by the method of B. I. Cook and Buckley (2009) (Text S2). To
 143 match the proxies' time span, we finally used the streamflow data from November 1921
 144 to October 2005.

2.4 Proxy–Streamflow Correlations

As a preliminary investigation, we performed correlation analyses between streamflow and proxy data. Correlations are calculated at different lags: $l = -2$ to $+2$ years. Negative lags account for the case when trees use stored carbon from previous years, and positive lags for the case when the catchment’s runoff processes are slower than precipitation inputs (Stockton & Jacoby, 1976; Meko et al., 2007). For robustness, we repeated the correlation analysis 1,000 times using the stationary bootstrap (Politis & Romano, 1994). In the following discussion we refer to the median bootstrap correlations (Figure 2).

Among the ring width sites, there are multiple correlation patterns (Figure 2a): some sites such as Chin Hills and Phu Toei correlate positively, while others (e.g., Phou Khao Khouay) correlate negatively. Peculiarly, the Mae Hong Son site displays significant negative correlation at $l = -2$ but significant positive correlations at $l = 0$ and $l = 2$. Five sites do not correlate with streamflow at all. These various patterns suggest that the ring width–streamflow relationship is complex and “noisy”. A large number of sites are thus required to extract the strongest signals.

Unlike ring width, $\delta^{18}\text{O}$ displays more consistent correlation patterns (Figure 2b): all significant correlations are negative, and the strongest correlations are often observed at $l = 0$. Some correlations have magnitudes larger than 0.5, while the largest correlation magnitude in ring width is only 0.36. These observations corroborate that $\delta^{18}\text{O}$ chronologies may contain stronger climate signals than do ring width chronologies (C. Xu et al., 2019; Gagen et al., 2011).

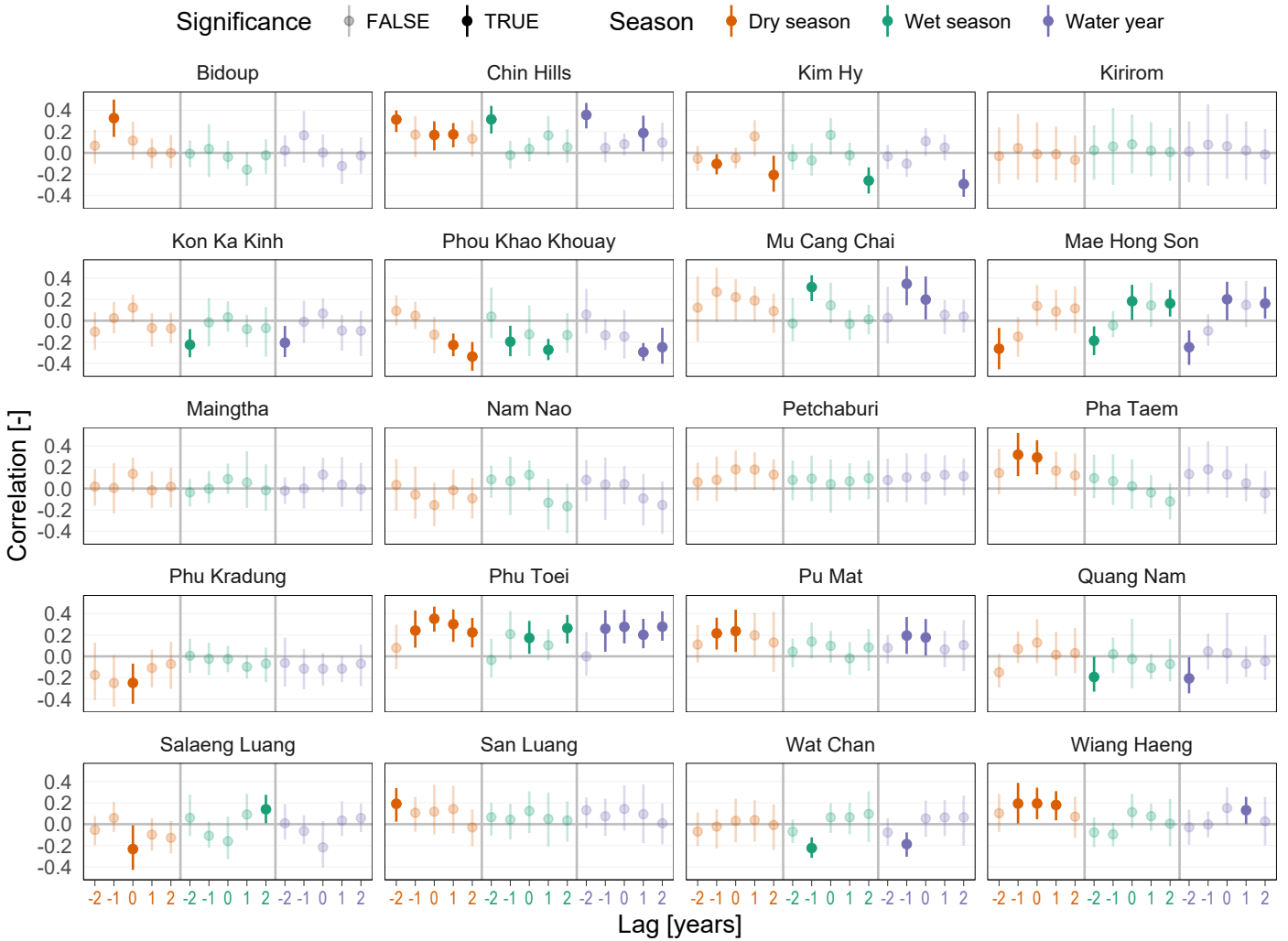
In general, we observe that ring width tends to correlate more strongly with dry season flow than with wet season flow. Conversely, $\delta^{18}\text{O}$ tends to correlate more strongly with wet season flow than with dry season flow. Both proxies correlate well with annual flow. The proxy–streamflow correlations observed here are also in agreement with the proxy–precipitation correlation analysis (Text S5). Both analyses show that tree ring proxies have different strength and sensitivity to different parts of the hydrograph, and have the potential to be combined for better seasonal reconstructions.

3 Reconstruction Framework

The correlation analysis shows diverse seasonal sensitivity among proxy chronologies and at different lags. To build reconstruction models, we define an *input* as a chronology–lag combination that significantly correlates with streamflow. For instance, some inputs for the annual reconstruction are Chin Hills ring-width at lag -2, and Umpang $\delta^{18}\text{O}$ at lag 0 (Figure 2).

The reconstruction framework consists of two main modules: Regression and Input Selection. In Regression (Section 3.1), the selected inputs for each target are given, and we find the regression coefficients that best match the targets while accounting for mass balance simultaneously, using a *penalized least squares* formulation. In Input Selection (Section 3.2), we find the best subset of inputs that minimizes the penalized least

a) Correlations between ring width and instrumental + naturalized streamflow



b) Correlations between $\delta^{18}\text{O}$ and instrumental + naturalized streamflow

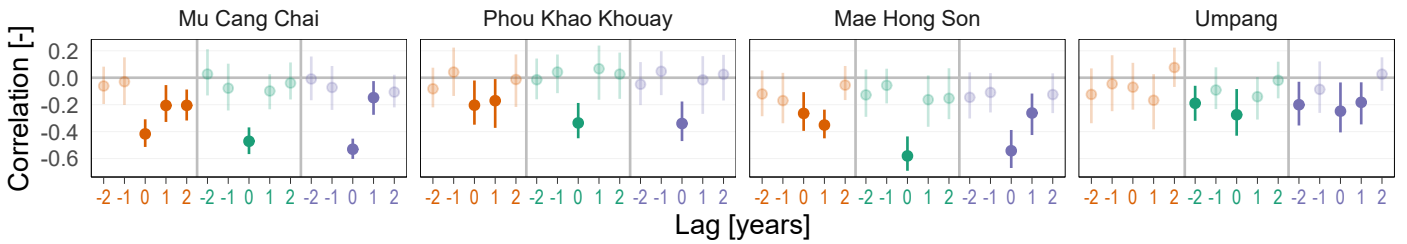


Figure 2. Streamflow–proxy correlations. The error bars show the 5th–95th bootstrapped empirical quantiles obtained from 1,000 replicates, using the stationary bootstrap (Politis & Romano, 1994). The dots indicate the medians. Lag l denotes correlations between proxy at year t and streamflow at year $t + l$.

185 squares. The two modules are unified in a nested optimization framework that includes
 186 a rigorous cross-validation scheme to assess reconstruction skills (Section 3.3).

187 3.1 Mass-balance-adjusted Regression

188 Assume that we have a matrix \mathbf{U}_d whose columns contain the selected inputs for
 189 the dry season. We first need to remove multicollinearity within \mathbf{U}_d . A common approach
 190 in dendrohydrology is to perform Principal Component Analysis (PCA) on \mathbf{U}_d , then re-
 191 duce the set of principal components (PCs) to a parsimonious subset that is most rel-
 192 evant to the streamflow target (Hidalgo et al., 2000; Coulthard et al., 2016). Here, we
 193 use a backward stepwise PC selection routine (Woodhouse et al., 2006). This transfor-
 194 mation from the selected inputs to the selected PCs is denoted as the function $g(\cdot)$:

$$195 \quad \mathbf{X}_d = g(\mathbf{U}_d) \quad (1)$$

196 Similarly, given the selected inputs \mathbf{U}_w for the wet season and \mathbf{U}_q for the water year,
 197 we apply $g(\cdot)$ to get

$$198 \quad \mathbf{X}_w = g(\mathbf{U}_w) \quad (2)$$

$$199 \quad \mathbf{X}_q = g(\mathbf{U}_q) \quad (3)$$

200 Now, let $\mathbf{y}_d, \mathbf{y}_w$, and \mathbf{y}_q be the target time series of dry season, wet season, and
 201 annual streamflow, respectively (these targets can be log-transformed when necessary).
 202 Reconstructing streamflow for the three targets means solving the following regression
 203 equations:

$$204 \quad \mathbf{y}_d = \mathbf{X}_d \boldsymbol{\beta}_d + \boldsymbol{\varepsilon}_d \quad (4)$$

$$205 \quad \mathbf{y}_w = \mathbf{X}_w \boldsymbol{\beta}_w + \boldsymbol{\varepsilon}_w \quad (5)$$

$$206 \quad \mathbf{y}_q = \mathbf{X}_q \boldsymbol{\beta}_q + \boldsymbol{\varepsilon}_q \quad (6)$$

207 where $\boldsymbol{\beta}_d, \boldsymbol{\beta}_w$, and $\boldsymbol{\beta}_q$ are the corresponding regression coefficients; and $\boldsymbol{\varepsilon}_d, \boldsymbol{\varepsilon}_w$, and $\boldsymbol{\varepsilon}_q$
 208 are white noise.

209 Next, let

$$210 \quad \mathbf{y} = \begin{bmatrix} \mathbf{y}_d \\ \mathbf{y}_w \\ \mathbf{y}_q \end{bmatrix}, \quad \mathbf{X} = \begin{bmatrix} \mathbf{X}_d & & \\ & \mathbf{X}_w & \\ & & \mathbf{X}_q \end{bmatrix}, \quad \boldsymbol{\beta} = \begin{bmatrix} \boldsymbol{\beta}_d \\ \boldsymbol{\beta}_w \\ \boldsymbol{\beta}_q \end{bmatrix}, \quad \text{and} \quad \boldsymbol{\varepsilon} = \begin{bmatrix} \boldsymbol{\varepsilon}_d \\ \boldsymbol{\varepsilon}_w \\ \boldsymbol{\varepsilon}_q \end{bmatrix}. \quad (7)$$

211 Equations 4–6 can then be converted to a more compact form

$$212 \quad \mathbf{y} = \mathbf{X}\boldsymbol{\beta} + \boldsymbol{\varepsilon}. \quad (8)$$

213 Equation 8 has the canonical form of linear regression. It can be solved as a least-squares
 214 problem:

$$215 \quad \min_{\boldsymbol{\beta}} J_1 = (\mathbf{y} - \mathbf{X}\boldsymbol{\beta})'(\mathbf{y} - \mathbf{X}\boldsymbol{\beta}), \quad (9)$$

216 yielding the solution

$$217 \quad \boldsymbol{\beta} = (\mathbf{X}'\mathbf{X})^{-1}\mathbf{X}'\mathbf{y}. \quad (10)$$

218 Solving Equation 8 is equivalent to solving Equations 4–6 simultaneously. The three re-
 219 gression problems in Equations 4–6 are independent of one another, and the above for-
 220 mulation places no constraints to match the sum of the seasonal flows to the annual flow.
 221 Therefore, such formulation can yield large differences in the annual mass balance. As
 222 we shall see later, this happens at station P.1.

223 To account for mass balance, it is tempting to impose a constraint,

$$224 \quad \mathbf{X}_d\boldsymbol{\beta}_d + \mathbf{X}_w\boldsymbol{\beta}_w = \mathbf{X}_q\boldsymbol{\beta}_q. \quad (11)$$

225 But, Equation 11 is often overdetermined: it is a system of T equations, one for each year,
 226 and we almost always have more equations than unknowns in a regression problem. In-
 227 stead, we can add to the objective function in Equation 9 a penalty term that is based
 228 on the differences ($\boldsymbol{\delta}$) between the LHS and the RHS of Equation 11.

$$229 \quad \boldsymbol{\delta} = \mathbf{X}_d\boldsymbol{\beta}_d + \mathbf{X}_w\boldsymbol{\beta}_w - \mathbf{X}_q\boldsymbol{\beta}_q. \quad (12)$$

230 If the reconstructions involve log-transformed flows, the mass difference is

$$231 \quad \delta_t = \log\left(\exp(\mathbf{x}_{d,t}\boldsymbol{\beta}_d) + \exp(\mathbf{x}_{w,t}\boldsymbol{\beta}_w)\right) - \mathbf{x}_{q,t}\boldsymbol{\beta}_q \quad \forall t = 1, \dots, T. \quad (13)$$

232 Just as we minimize the squared differences between prediction and observation, we also
 233 minimize the squared mass differences. Finally, we add a weight λ to represent the im-
 234 portance of the penalty term, and obtain a new objective function

$$235 \quad \min_{\boldsymbol{\beta}} J_2 = (\mathbf{y} - \mathbf{X}\boldsymbol{\beta})'(\mathbf{y} - \mathbf{X}\boldsymbol{\beta}) + \lambda\boldsymbol{\delta}'\boldsymbol{\delta} \quad (14)$$

236 We call this the *penalized least squares* problem. Observe that when $\lambda = 0$, the penalty
 237 term disappears, and the penalized least squares problem becomes the canonical least
 238 squares problem. The higher λ is, the more important the penalty becomes.

239 Without flow transformation, $\boldsymbol{\delta}$ is linear (Equations 12), so J_2 is quadratic. We can
 240 solve Equation 14 analytically to get

$$241 \quad \boldsymbol{\beta} = (\mathbf{X}'\mathbf{X} + \lambda\mathbf{A}'\mathbf{A})^{-1}\mathbf{X}'\mathbf{y} \quad (15)$$

242 where $\mathbf{A} = [\mathbf{X}_d \quad \mathbf{X}_w \quad -\mathbf{X}_q]$. The proof is provided in Text S6.

243 When log-transformations are involved, $\boldsymbol{\delta}$ is not linear, and Equation 14 cannot be
 244 solved analytically. But it can be solved numerically using any nonlinear solver. Here,
 245 we use an efficient quasi-Newton method called L-BFGS-B (Byrd et al., 1995), available
 246 in the R function `optim()`. We have implemented the mass-balance-adjusted regression
 247 procedure in the R package `mbr`, currently available on GitHub at [github.com/ntthung/](https://github.com/ntthung/mbr)
 248 `mbr`.

249 3.2 Optimal Input Selection

250 A consolidated approach to input selection in the literature is to use Branch and
 251 Bound algorithms, such as Leaps and Bounds (Furnival & Wilson, 1974) or its more re-
 252 cent variants (Duarte Silva, 2001, 2002). These algorithms are conceived to balance goodness-
 253 of-fit with model simplicity. In this work however, we also need to account for mass bal-
 254 ance besides goodness-of-fit. Therefore, the input selection routine must explicitly ac-
 255 count for the penalized least squares objective (Equation 14). If the number of inputs

256 is small, we can exhaustively search all possible subsets and choose the one that yields
 257 the minimum penalized least square value (PLSV). However, this method quickly be-
 258 comes infeasible with increasing input size: there are 2^n subsets of n inputs (for station
 259 P.1, $n = 19, 28,$ and 30). A computationally tractable optimization is necessary (Galelli
 260 et al., 2014).

261 We formulate input selection as a binary optimization problem. Each input has an
 262 index, and a binary vector \mathbf{p} encodes input selection: $p_i = 1$ means the i^{th} input is se-
 263 lected. For any given \mathbf{p} , i.e. for any given input subset, we can solve the mass-balance-
 264 adjusted regression problem to obtain a PLSV. Our goal then is to find \mathbf{p} that has the
 265 best PLSV over all \mathbf{p} 's.

266 Note that \mathbf{p} has three components: $\mathbf{p} = [\mathbf{d} \quad \mathbf{w} \quad \mathbf{q}]'$. Component \mathbf{d} represents the
 267 dry season:

$$268 \quad d_i = \begin{cases} 1 & \text{if proxy } i \text{ is used for the dry season} \\ 0 & \text{otherwise} \end{cases} \quad i = 1, \dots, n_d. \quad (16)$$

269 So, where $d_i = 1$, we take the i^{th} inputs and place into the matrix \mathbf{U}_d . Similarly, we
 270 create \mathbf{U}_w from \mathbf{w} and \mathbf{U}_q from \mathbf{q} . Once we have \mathbf{U}_d , \mathbf{U}_w , and \mathbf{U}_q , the mass-balance-
 271 adjusted regression procedure can be applied. To improve the robustness of the input
 272 selection, the regression is cross-validated 50 times (Section 3.3), each yields one PLSV
 273 estimate. The average of all runs, denoted $f(\mathbf{p})$, is used as the final PLSV for \mathbf{p} .

274 The remaining task is to solve

$$275 \quad \min_{\mathbf{p}} f(\mathbf{p}). \quad (17)$$

276 We solve Equation 17 with Genetic Algorithm (Holland, 1975), a metaheuristic op-
 277 timization technique that allows us to treat the underlying regression as a black-box while
 278 searching for the best subset of inputs (Kohavi & John, 1997), and is well suited for bi-
 279 nary optimization (Whitley, 1994). We use the R package GA (Scrucca, 2013). Details
 280 about the implementations are provided in Text S8.

281 3.3 Model Assessment

282 We set up a reconstruction experiment involving two models: Model 0 runs with-
 283 out the mass balance adjustment ($\lambda = 0$ in Equation 14) and Model 1 has the adjust-
 284 ment ($\lambda = 1$). Other than the different values for λ , both models are trained exactly
 285 the same way, following Sections 3.1 and 3.3.

286 During optimization, multiple reconstructions are created while the optimal \mathbf{p} is
 287 sought for each model. These reconstructions are assessed with the PLSV. The final re-
 288 constructions, created with the optimal inputs, are further assessed post hoc with the
 289 commonly used metrics: coefficient of determination (R^2), reduction of error (RE), and
 290 coefficient of efficiency (CE) (Nash & Sutcliffe, 1970; Fritts, 1976). All metrics are cal-
 291 culated over 50 cross-validation runs.

292 Following Nguyen et al. (2020), we adopt a leave-25%-out cross-validation scheme,
 293 where each hold-out chunk is contiguous. The contiguous chunks aim to test whether

294 the reconstruction can capture regimes in the time series, in line with the traditional split-
 295 sample scheme. The 50 repetitions provide a distribution for each skill metric, allowing
 296 more robust estimation of the mean skill score. More importantly, the distributions enable
 297 us to assess the statistical significance of skills. For example, a reconstruction is con-
 298 sidered statistically skillful with respect to CE at $\alpha = 0.1$ if the probability of nega-
 299 tive CE is less than 0.1.

300 4 Results

301 4.1 Reconstructions

302 For Model 0’s dry season and annual reconstructions, all metrics are at least 0.40,
 303 and the reconstructions match their targets closely (Figure 3a). Furthermore, these re-
 304 constructions are statistically skillful at $\alpha = 0.1$. Conversely, Model 0’s wet season re-
 305 construction is not statistically skillful. Although the mean RE and CE are positive (RE
 306 = 0.35, CE = 0.23), these scores vary widely over the cross-validation runs (Figure S12),
 307 suggesting that the wet season reconstruction is sensitive to training data. The large vari-
 308 ability of skills is also consistent with the high variability of streamflow (Figure S5). These
 309 observations suggest that there may be nonlinearity in the streamflow–proxy relation-
 310 ships at the extremes. In future studies, nonlinear reconstruction models (e.g., Nguyen
 311 & Galelli, 2018) could be incorporated to address this problem.

312 Model 1, with the penalty term, makes visible adjustments to the seasonal recon-
 313 structions but minimal changes to the annual one for the instrumental period (Figure
 314 3a). Dry season skills slightly decrease, wet season’s RE and CE increase, and annual
 315 skills remain almost the same. While the mean skill scores of both models are similar,
 316 Model 1 produces notably narrower distributions of RE and CE for the wet season (Fig-
 317 ure S12). Consequently, Model 1’s wet season reconstruction becomes statistically skill-
 318 ful. Overall, Model 1 is more robust.

319 To understand Model 1’s robustness, let us recall the models’ formulation. Model
 320 0 reconstructs the dry season, wet season, and annual flows independently. Each recon-
 321 struction is geared towards its own target, and can become sensitive to training data—
 322 the wet season reconstruction does. Contrarily, Model 1 links all three reconstructions
 323 together via the penalty term (Equations 12–14). This link provides each reconstruction
 324 with additional information from the other two, thus preventing each reconstruction from
 325 overfitting to its own target. In our case, the wet season reconstruction benefited sig-
 326 nificantly from this additional information to become statistically skillful, with minimal
 327 trade-off from the other two reconstructions.

328 The selected input subsets by both models provide further insights into their simi-
 329 larities and differences. Both models use similar input subsets, with identical ones for
 330 the water year. However, Model 1 uses fewer inputs than does Model 0 for the wet and
 331 dry seasons (Figure 4). Therefore, the models behave similarly, but Model 1 is more par-
 332 simonious.

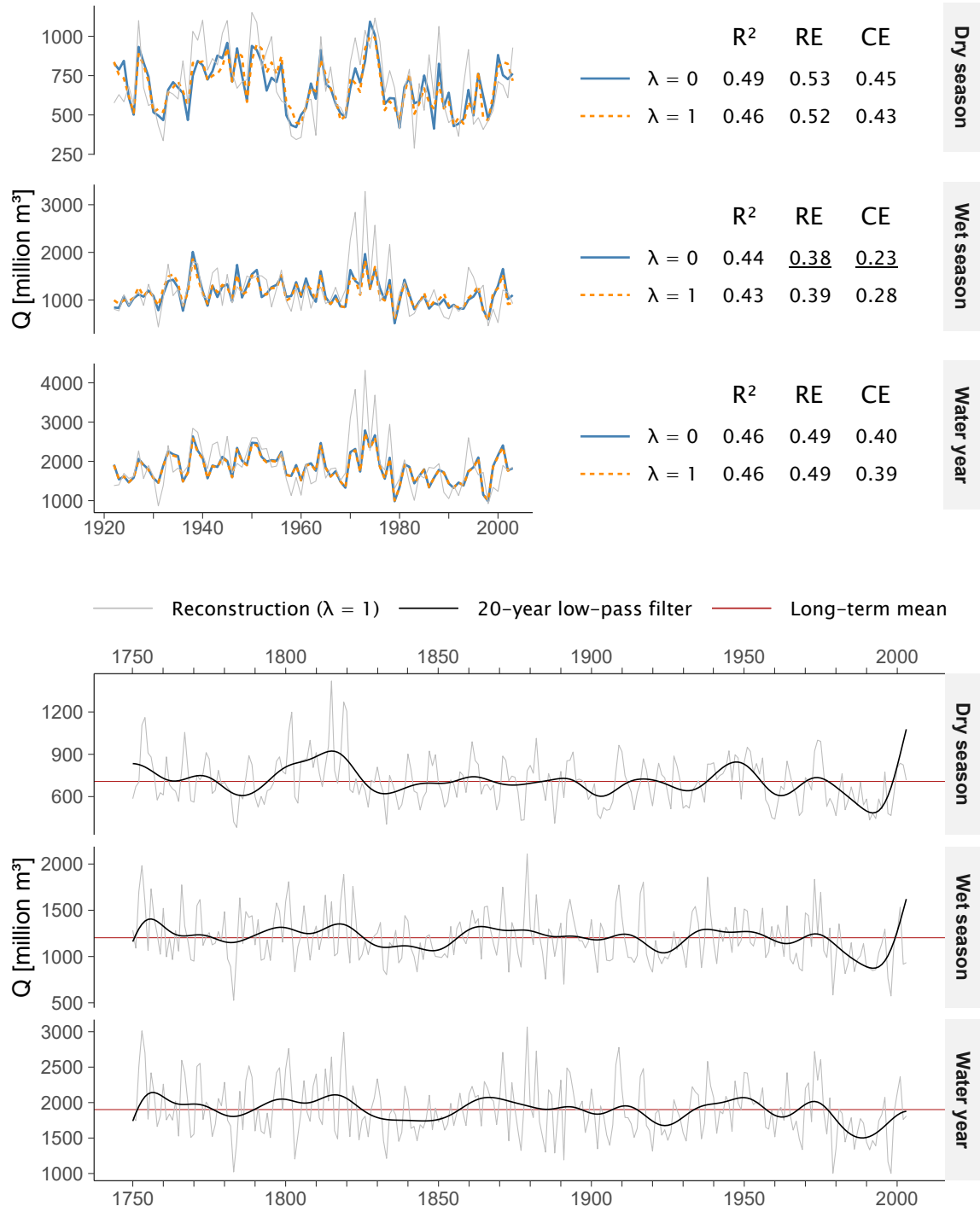


Figure 3. (a) Reconstruction skills and time series for the instrumental period, produced using two models: without mass balance penalty ($\lambda = 0$) and with penalty ($\lambda = 1$) in the regression problem (Equation 14). Grey lines show naturalized observations. Underlined scores show where the reconstruction is not statistically skillful at $\alpha = 0.1$. (b) Full reconstructions with $\lambda = 1$.

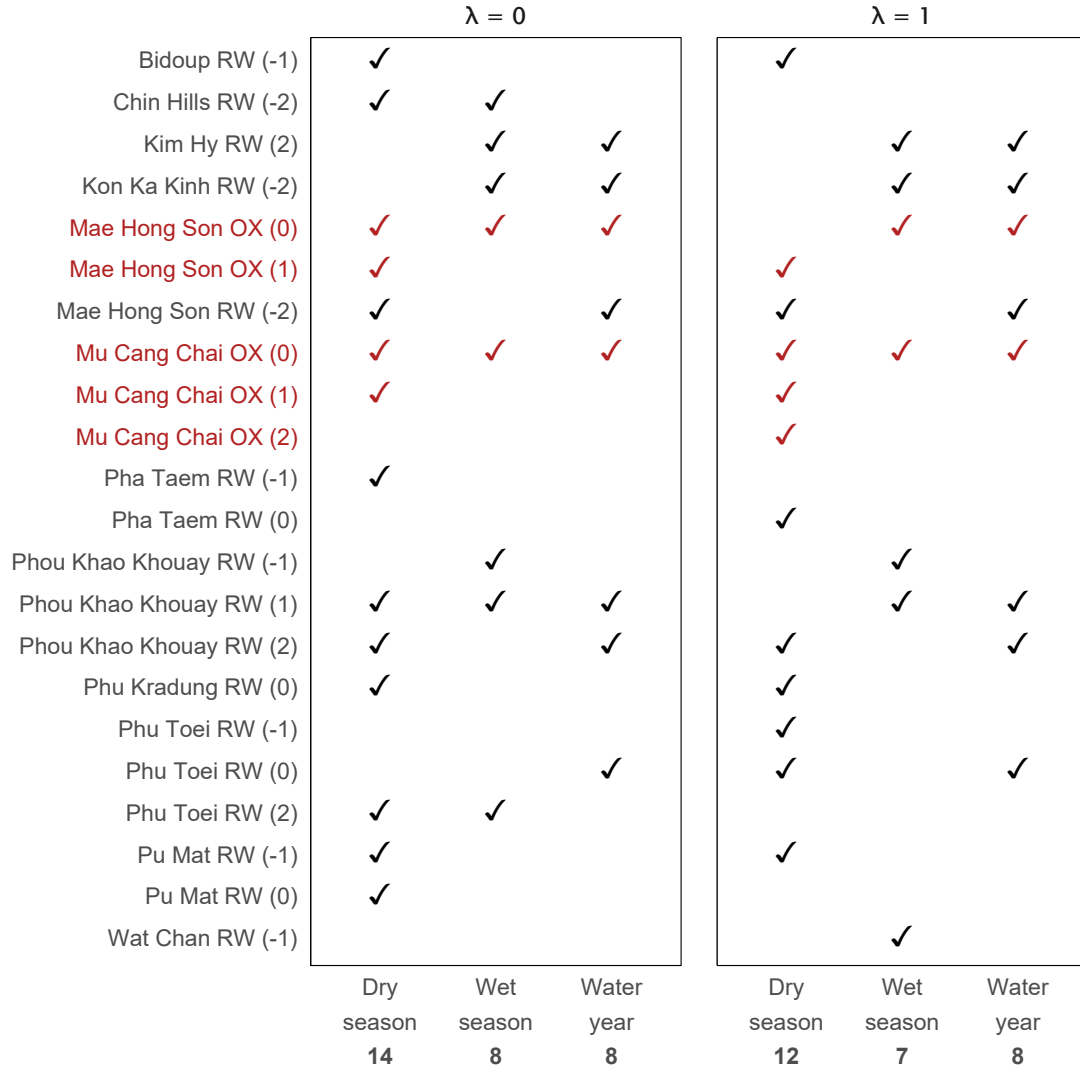


Figure 4. Selected inputs for each streamflow target (columns) in each models (panels). Only inputs that were selected at least once are shown. The stable oxygen isotope (OX) inputs are marked in dark red. Bold numbers at the bottom row of the x-axis are the number of selected inputs in each column.

333 Surprisingly, the Mu Cang Chai and Mae Hong Son $\delta^{18}\text{O}$ chronologies were con-
 334 sistently selected by both models for all reconstructions, including the dry season recon-
 335 structions where we expected ring width chronologies to dominate, based on the observed
 336 tendencies of ring width to correlate more with wet season flow and $\delta^{18}\text{O}$ to correlate
 337 more with dry season flow. Upon closer examinations of the correlation analysis (Fig-
 338 ure 2), the puzzle is solved. First, the $\delta^{18}\text{O}$ chronologies are intercorrelated (C. Xu et
 339 al., 2019), and the input selection algorithm correctly selected the two sites that exhibit
 340 the strongest correlations. Second, while these $\delta^{18}\text{O}$ chronologies correlate less with dry

341 season flow than they do with wet season flow, the correlations are still stronger than
 342 those observed at many ring width sites.

343 Over the whole study horizon, we observe similar results to those of the instrumen-
 344 tal period (Figure S13). The two models agree with each other. Model 1's adjustments
 345 are generally small. The largest adjustments are in the wet season ($\pm 400 \text{ Mm}^3$); smaller
 346 but notable adjustments are seen in the dry season ($\pm 200 \text{ Mm}^3$), and minute adjustments
 347 ($< 90 \text{ Mm}^3$) are seen in the annual reconstruction. We will examine the effects of these
 348 adjustments in Section 4.2.

349 The reconstructions provide some interesting insights into the inter- and intra-annual
 350 variability of the river (Figure 3b). Between 1825–1855, sustained low flow was observed
 351 in the wet season and water year reconstructions. However, in the dry season, the low
 352 flow period ended 15 years earlier, around 1840. Conversely, a period of sustained high
 353 flow was observed in all three reconstructions between 1790–1820, especially for the dry
 354 season. Most notably, dry season flow in 1815 was so high that it accounted for more than
 355 50% of the annual flow—a rare event that occurred in only 8 of 254 years (Figure S14,
 356 see also Text S9).

357 4.2 Annual Mass Balance

358 For each model, we compare the total seasonal flow with the annual flow. To pre-
 359 serve the annual mass balance, these two time series should ideally be the same. How-
 360 ever, for Model 0, large discrepancies are seen between the two time series (Figure 5a).
 361 For Model 1, the two time series agree with each other better. As each time series pro-
 362 vides an estimate of the annual water budget, we are also interested in their distribu-
 363 tions. We observe that the distributions produced by Model 0 are notably different from
 364 each other, but those produced by Model 1 are almost identical (Figure 5b). This im-
 365 plies that the distributions derived from Model 1 are more reliable. Using the same anal-
 366 ysis, we show that Model 1 also produces more reliable distributions of the dry and wet
 367 season's water budget than does Model 0 (Figure S15).

368 Next, for each model, we calculate the mass difference, ΔQ , between the total sea-
 369 sonal flow and the annual flow, then examine its trajectory and distribution (Figures 5c
 370 and 5d). The mass difference for Model 0 ranges from -640 Mm^3 to 600 Mm^3 , while that
 371 range for Model 1 is -270 Mm^3 to 370 Mm^3 ; a 50% reduction in range. Moreover, Model
 372 0 yields a mass difference outside the interval $\pm 190 \text{ Mm}^3$ ($\pm 10\%$ of the mean annual flow;
 373 shaded region in Figure 5d) in 28% of the years. That figure for Model 1 is only 11%.
 374 By these metrics, Model 1 is twice better than Model 0 in terms of preserving mass bal-
 375 ance.

376 5 Discussion and Conclusions

377 In Section 4.1, we showed that the optimal input selection procedure yields good
 378 reconstruction skills for both model setups, and that Model 1, by imposing a mass bal-
 379 ance adjustment, produces more robust reconstructions than does Model 0. More im-

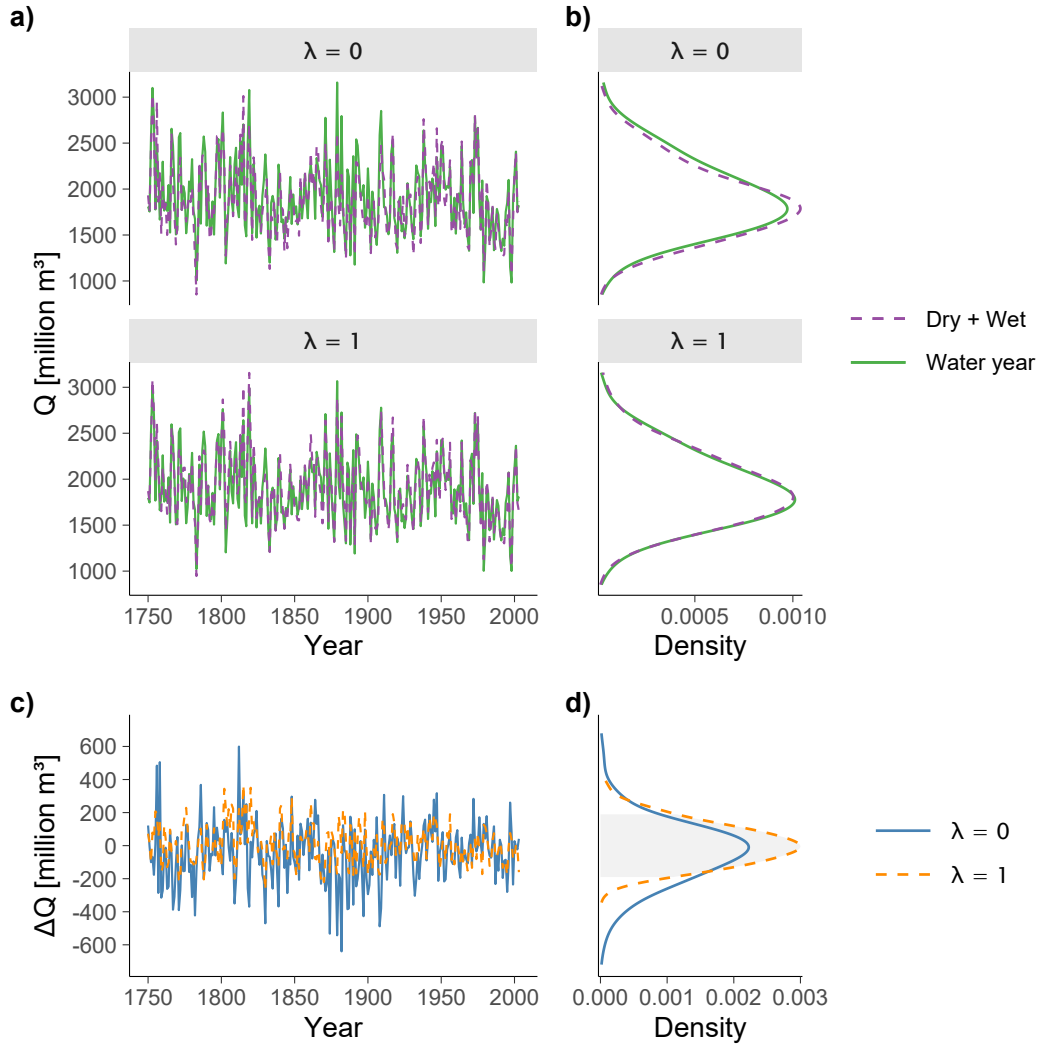


Figure 5. (a) Comparison between the total seasonal flow (TSF; Wet + Dry) and the annual flow (AF; Water year) for Model 0 ($\lambda = 0$) and Model 1 ($\lambda = 1$). (b) Distributions of the annual water budget, estimated by either the TSF or the AF for both models. (c) The differences, ΔQ , between the TSF and the AF. (d) Distributions of ΔQ . The shaded region denotes the ± 190 Mm^3 range, equivalent to $\pm 10\%$ of the mean annual flow.

380 portantly, the adjustment significantly reduces the differences between the total seasonal
 381 flow and the annual flow (Section 4.2). Without the adjustment, the mass difference can
 382 be as large as 640 Mm^3 , or about 30% of the mean annual flow. It amounts to 90% of
 383 the irrigation demand from the Ping River downstream of Bhumibol Reservoir (Divakar
 384 et al., 2011). Such a discrepancy may lead to water allocation disputes. With the ad-
 385 justment, both the frequency and magnitude of discrepancies are reduced—this is cru-
 386 cial for water availability assessment, a major goal of dendrohydrology.

387 We also showed that the mass-balanced-adjusted regression produces reliable dis-
 388 tributions of the seasonal and annual streamflow. These distributions can be used for
 389 probabilistic studies in water resources applications. For example, sub-annual stochas-
 390 tic time series can be generated from the distributions to be used in bottom-up vulner-
 391 ability assessments of water systems (Pielke et al., 2012; Herman et al., 2016). In Text
 392 S10 we illustrate one simple way to do so (by sampling from a bivariate distribution fit-
 393 ted to the seasonal reconstructions), but more advanced methods are available (e.g., Bor-
 394 gomeo, Farmer, & Hall, 2015; Borgomeo, Pflug, et al., 2015).

395 The framework that we proposed here can be reapplied and expanded in several
 396 ways. First, analysts adopting our framework have the choice to tune λ , depending on
 397 how important it is to preserve mass balance in their applications. In this case, a sen-
 398 sitivity analysis with respect to λ may be informative. Second, the mass balance formu-
 399 lation is applicable to other climate variables such as precipitation, and to other contexts
 400 where a penalty term in the regression equation is desirable. For example, if one wishes
 401 to reconstruct streamflow at two tributaries as well as the main stream of a river, the
 402 mass balance adjustment should be used to minimize the difference between the total
 403 flow of the tributaries and the flow on the main stream. Finally, the mass balance for-
 404 mulation is readily extendable to higher resolutions, e.g., quarterly or monthly (Text S7),
 405 as long as the proxy network is sensitive enough to the higher resolution targets. These
 406 directions can help dendrohydrology realize its value in operational water management,
 407 an area where annual, unconstrained streamflow reconstructions have had limited suc-
 408 cess.

409 Acknowledgments

410 We are indebted to Edward Cook for the updated chronologies (Salaeng Luang, Mae Hong
 411 Son, and Mu Cang Chai), and for his valuable comments. We are also grateful to Thanh
 412 Dang for the VIC-Res model output. The diligent work of Le Canh Nam and many other
 413 local colleagues in collecting tree core samples over many years is crucial in building the
 414 tree ring network, and is sincerely appreciated. We knew of Hardman and Reil (1936)
 415 through Adam Csank’s presentation at AAG 2019. Nguyen Tan Thai Hung is supported
 416 by the President’s Graduate Fellowship from the Singapore University of Technology and
 417 Design. Chenxi Xu is supported by the Chinese Academy of Sciences (CAS) Pioneer Hun-
 418 dred Talents Program.

419 References

- 420 Borgomeo, E., Farmer, C. L., & Hall, J. W. (2015, jul). Numerical rivers: A syn-
 421 thetic streamflow generator for water resources vulnerability assessments. *Wa-*
 422 *ter Resources Research*, 51(7), 5382–5405. DOI: 10.1002/2014WR016827
- 423 Borgomeo, E., Pflug, G., Hall, J. W., & Hochrainer-Stigler, S. (2015, nov). Assessing
 424 water resource system vulnerability to unprecedented hydrological drought
 425 using copulas to characterize drought duration and deficit. *Water Resources*
 426 *Research*, 51(11), 8927–8948. DOI: 10.1002/2015WR017324
- 427 Buckley, B. M., Anchukaitis, K. J., Penny, D., Fletcher, R., Cook, E. R., Sano, M.,

- 428 ... Hong, T. M. (2010, apr). Climate as a contributing factor in the demise of
 429 Angkor, Cambodia. *Proceedings of the National Academy of Sciences*, *107*(15),
 430 6748–6752. DOI: 10.1073/pnas.0910827107
- 431 Buckley, B. M., Barbetti, M., Watanasak, M., Arrigo, R. D., Boonchirdchoo, S., &
 432 Sarutanon, S. (1995, feb). Dendrochronological Investigations in Thailand.
 433 *IAWA Journal*, *16*(4), 393–409. DOI: 10.1163/22941932-90001429
- 434 Buckley, B. M., Duangsathaporn, K., Palakit, K., Butler, S., Syhapanya, V., &
 435 Xaybouangeun, N. (2007, dec). Analyses of growth rings of *Pinus merkusii*
 436 from Lao P.D.R. *Forest Ecology and Management*, *253*(1-3), 120–127. DOI:
 437 10.1016/j.foreco.2007.07.018
- 438 Buckley, B. M., Fletcher, R., Wang, S. Y. S., Zottoli, B., & Pottier, C. (2014).
 439 Monsoon extremes and society over the past millennium on main-
 440 land Southeast Asia. *Quaternary Science Reviews*, *95*, 1–19. DOI:
 441 10.1016/j.quascirev.2014.04.022
- 442 Buckley, B. M., Palakit, K., Duangsathaporn, K., Sanguantham, P., & Prasomsin,
 443 P. (2007). Decadal scale droughts over northwestern Thailand over the past
 444 448 years: Links to the tropical Pacific and Indian Ocean sectors. *Climate*
 445 *Dynamics*, *29*(1), 63–71. DOI: 10.1007/s00382-007-0225-1
- 446 Buckley, B. M., Stahle, D. K., Luu, H. T., Wang, S. Y., Nguyen, T. Q. T., Thomas,
 447 P., ... Nguyen, V. T. (2017). Central Vietnam climate over the past five cen-
 448 turies from cypress tree rings. *Climate Dynamics*, *48*(11-12), 3707–3723. DOI:
 449 10.1007/s00382-016-3297-y
- 450 Buckley, B. M., Ummenhofer, C. C., D’Arrigo, R. D., Hansen, K. G., Truong, L. H.,
 451 Le, C. N., & Stahle, D. K. (2019, sep). Interdecadal Pacific Oscillation re-
 452 constructed from trans-Pacific tree rings: 1350–2004 CE. *Climate Dynamics*,
 453 *53*(5-6), 3181–3196. DOI: 10.1007/s00382-019-04694-4
- 454 Byrd, R. H., Lu, P., Nocedal, J., & Zhu, C. (1995, sep). A Limited Memory Algo-
 455 rithm for Bound Constrained Optimization. *SIAM Journal on Scientific Com-*
 456 *puting*, *16*(5), 1190–1208. DOI: 10.1137/0916069
- 457 Cook, B. I., & Buckley, B. M. (2009, dec). Objective determination of monsoon sea-
 458 son onset, withdrawal, and length. *Journal of Geophysical Research*, *114*(D23),
 459 D23109. DOI: 10.1029/2009JD012795
- 460 Cook, E. R., Anchukaitis, K. J., Buckley, B. M., D’Arrigo, R. D., Jacoby, G. C.,
 461 & Wright, W. E. (2010, apr). Asian Monsoon Failure and Megadrought
 462 During the Last Millennium. *Science*, *328*(5977), 486–489. DOI:
 463 10.1126/science.1185188
- 464 Coulthard, B., Smith, D. J., & Meko, D. M. (2016, mar). Is worst-case scenario
 465 streamflow drought underestimated in British Columbia? A multi-century per-
 466 spective for the south coast, derived from tree-rings. *Journal of Hydrology*,
 467 *534*, 205–218. DOI: 10.1016/j.jhydrol.2015.12.030
- 468 D’Arrigo, R., Abram, N. J., Ummenhofer, C., Palmer, J., & Mudelsee, M. (2011,
 469 feb). Reconstructed streamflow for Citarum River, Java, Indonesia: linkages
 470 to tropical climate dynamics. *Climate Dynamics*, *36*(3-4), 451–462. DOI:
 471 10.1007/s00382-009-0717-2

- 472 D'Arrigo, R., Barbett, M., Watanasak, M., Buckley, B. M., Krusic, P., Boonchird-
 473 choo, S., & Sarutanon, S. (1997, jan). Progress in Dendroclimatic Studies of
 474 Mountain Pine in Northern Thailand. *IAWA Journal*, *18*(4), 433–444. DOI:
 475 10.1163/22941932-90001508
- 476 D'Arrigo, R., Palmer, J., Ummenhofer, C. C., Kyaw, N. N., & Krusic, P. (2011).
 477 Three centuries of Myanmar monsoon climate variability inferred from
 478 teak tree rings. *Geophysical Research Letters*, *38*(24), 1–5. DOI:
 479 10.1029/2011GL049927
- 480 Divakar, L., Babel, M., Perret, S., & Gupta, A. D. (2011, apr). Optimal allocation of
 481 bulk water supplies to competing use sectors based on economic criterion – An
 482 application to the Chao Phraya River Basin, Thailand. *Journal of Hydrology*,
 483 *401*(1-2), 22–35. DOI: 10.1016/j.jhydrol.2011.02.003
- 484 Duarte Silva, A. P. (2001, jan). Efficient Variable Screening for Multivari-
 485 ate Analysis. *Journal of Multivariate Analysis*, *76*(1), 35–62. DOI:
 486 10.1006/jmva.2000.1920
- 487 Duarte Silva, A. P. (2002, nov). Discarding variables in a Principal Component
 488 Analysis: Algorithms for all-subsets comparisons. *Computational Statistics*,
 489 *17*(2), 251–271. DOI: 10.1007/s001800200105
- 490 Fritts, H. C. (1976). *Tree Rings and Climate*. London: Elsevier. DOI:
 491 10.1016/B978-0-12-268450-0.X5001-0
- 492 Fritts, H. C., Blasing, T. J., Hayden, B. P., & Kutzbach, J. E. (1971, oct). Multi-
 493 variate Techniques for Specifying Tree-Growth and Climate Relationships and
 494 for Reconstructing Anomalies in Paleoclimate. *Journal of Applied Meteorology*,
 495 *10*(5), 845–864. DOI: 10.1175/1520-0450(1971)010<0845:MTFSTG>2.0.CO;2
- 496 Furnival, G. M., & Wilson, R. W. (1974). Regressions by leaps and bounds. *Techno-*
 497 *metrics*, *16*(4), 499–511. DOI: 10.1080/00401706.1974.10489231
- 498 Gagen, M., McCarroll, D., Loader, N. J., & Robertson, I. (2011). Stable Iso-
 499 topes in Dendroclimatology: Moving Beyond ‘Potential’. In M. K. Hughes,
 500 T. W. Swetnam, & H. F. Diaz (Eds.), *Dendroclimatology: Progress and*
 501 *prospects* (pp. 147–172). Dordrecht: Springer Netherlands. DOI:
 502 10.1007/978-1-4020-5725-0_6
- 503 Galelli, S., Humphrey, G. B., Maier, H. R., Castelletti, A., Dandy, G. C., & Gibbs,
 504 M. S. (2014, dec). An evaluation framework for input variable selection algo-
 505 rithms for environmental data-driven models. *Environmental Modelling and*
 506 *Software*, *62*, 33–51. DOI: 10.1016/j.envsoft.2014.08.015
- 507 Güner, H. T., Köse, N., & Harley, G. L. (2017). A 200-year reconstruction of Ko-
 508 casu River (Sakarya River Basin, Turkey) streamflow derived from a tree-ring
 509 network. *International Journal of Biometeorology*, *61*(3), 427–437. DOI:
 510 10.1007/s00484-016-1223-y
- 511 Hansen, K. G., Buckley, B. M., Zottoli, B., D'Arrigo, R. D., Nam, L. C., Van
 512 Truong, V., ... Nguyen, H. X. (2017, nov). Discrete seasonal hydroclimate
 513 reconstructions over northern Vietnam for the past three and a half centuries.
 514 *Climatic Change*, *145*(1-2), 177–188. DOI: 10.1007/s10584-017-2084-z
- 515 Hardman, G., & Reil, O. E. (1936). The Relationship between Tree-Growth and

- 516 Stream Runoff in the Truckee River Basin, California-Nevada. *Nevada Agricultural Experiment Station Bulletin No. 141*.
- 517
- 518 Herman, J. D., Zeff, H. B., Lamontagne, J. R., Reed, P. M., & Characklis,
519 G. W. (2016, nov). Synthetic Drought Scenario Generation to Support
520 Bottom-Up Water Supply Vulnerability Assessments. *Journal of*
521 *Water Resources Planning and Management*, 142(11), 04016050. DOI:
522 10.1061/(ASCE)WR.1943-5452.0000701
- 523 Hidalgo, H. G., Piechota, T. C., & Dracup, J. A. (2000, nov). Alternative principal
524 components regression procedures for dendrohydrologic reconstructions. *Water*
525 *Resources Research*, 36(11), 3241–3249. DOI: 10.1029/2000WR900097
- 526 Holland, J. H. (1975). *Adaptation In Natural and Artificial Systems*. Ann Arbor,
527 Michigan: The University of Michigan Press.
- 528 Josse, J., & Husson, F. (2016). missMDA: A Package for Handling Missing Values
529 in Multivariate Data Analysis. *Journal of Statistical Software*, 70(1). DOI:
530 10.18637/jss.v070.i01
- 531 Kohavi, R., & John, G. H. (1997, dec). Wrappers for feature subset selection. *Artifi-*
532 *cial Intelligence*, 97(1-2), 273–324. DOI: 10.1016/s0004-3702(97)00043-x
- 533 Lieberman, V. (2003). *Strange Parallels: Volume 1, Integration on the Mainland:*
534 *Southeast Asia in Global Context, c.800–1830*. Cambridge University Press.
535 Retrieved from <https://books.google.com.sg/books?id=-01JisWpJBEC>
- 536 Lieberman, V., & Buckley, B. M. (2012). *The impact of climate on South-*
537 *east Asia, circa 950-1820: New findings* (Vol. 46) (No. 5). DOI:
538 10.1017/S0026749X12000091
- 539 Meko, D. M., & Woodhouse, C. A. (2011). Application of Streamflow Reconstruc-
540 tion to Water Resources Management. In M. K. Hughes, T. W. Swetnam, &
541 H. F. Diaz (Eds.), *Dendroclimatology: Progress and prospects* (pp. 231–261).
542 Dordrecht: Springer Netherlands. DOI: 10.1007/978-1-4020-5725-0_8
- 543 Meko, D. M., Woodhouse, C. A., Baisan, C. A., Knight, T., Lukas, J. J., Hughes,
544 M. K., & Salzer, M. W. (2007, may). Medieval drought in the upper Col-
545 orado River Basin. *Geophysical Research Letters*, 34(10), L10705. DOI:
546 10.1029/2007GL029988
- 547 Nash, J. E., & Sutcliffe, J. V. (1970, apr). River flow forecasting through conceptual
548 models part I — A discussion of principles. *Journal of Hydrology*, 10(3), 282–
549 290. DOI: 10.1016/0022-1694(70)90255-6
- 550 Nguyen, H. T. T., & Galelli, S. (2018, mar). A Linear Dynamical Systems Ap-
551 proach to Streamflow Reconstruction Reveals History of Regime Shifts in
552 Northern Thailand. *Water Resources Research*, 54(3), 2057–2077. DOI:
553 10.1002/2017WR022114
- 554 Nguyen, H. T. T., Turner, S. W. D., Buckley, B. M., & Galelli, S. (2020, sep).
555 Coherent stream flow variability in Monsoon Asia over the past eight
556 centuries—links to oceanic drivers. *Water Resources Research*. DOI:
557 10.1029/2020WR027883
- 558 Pielke, R. A., Wilby, R., Niyogi, D., Hossain, F., Dairuku, K., Adegoke, J., ...
559 Suding, K. (2012). Dealing With Complexity and Extreme Events Using a

- 560 Bottom-Up, Resource-Based Vulnerability Perspective. In *Extreme events*
 561 *and natural hazards: The complexity perspective* (pp. 345–359). American
 562 Geophysical Union. DOI: 10.1029/2011GM001086
- 563 Politis, D. N., & Romano, J. P. (1994). The Stationary Bootstrap. *Jour-*
 564 *nal of the American Statistical Association*, 89(428), 1303–1313. DOI:
 565 10.1080/01621459.1994.10476870
- 566 Prairie, J., Nowak, K., Rajagopalan, B., Lall, U., & Fulp, T. (2008). A stochastic
 567 nonparametric approach for streamflow generation combining observational
 568 and paleoreconstructed data. *Water Resources Research*, 44(6), 1–11. DOI:
 569 10.1029/2007WR006684
- 570 Rao, M. P. (2020). *Hydroclimate variability and environmental change in Eurasia*
 571 *over the past millennium and its impacts* (PhD Thesis, Columbia University).
 572 DOI: 10.7916/d8-890y-wb66
- 573 Rao, M. P., Cook, E. R., Cook, B. I., Palmer, J. G., Uriarte, M., Devineni, N., ...
 574 Wahab, M. (2018, aug). Six Centuries of Upper Indus Basin Streamflow Vari-
 575 ability and Its Climatic Drivers. *Water Resources Research*, 54(8), 5687–5701.
 576 DOI: 10.1029/2018WR023080
- 577 Sano, M., Buckley, B. M., & Sweda, T. (2009). Tree-ring based hydroclimate recon-
 578 struction over northern Vietnam from *Fokienia hodginsii*: Eighteenth century
 579 mega-drought and tropical Pacific influence. *Climate Dynamics*, 33(2-3),
 580 331–340. DOI: 10.1007/s00382-008-0454-y
- 581 Sano, M., Xu, C., & Nakatsuka, T. (2012, jun). A 300-year Vietnam hydro-
 582 climate and ENSO variability record reconstructed from tree ring $\delta 18 O$.
 583 *Journal of Geophysical Research: Atmospheres*, 117(D12), D12115. DOI:
 584 10.1029/2012JD017749
- 585 Sauchyn, D., & Ilich, N. (2017, nov). Nine Hundred Years of Weekly Streamflows:
 586 Stochastic Downscaling of Ensemble Tree-Ring Reconstructions. *Water Re-*
 587 *sources Research*, 1–18. DOI: 10.1002/2017WR021585
- 588 Schulman, E. (1945). Tree-ring hydrology of the Colorado River Basin. *University*
 589 *of Arizona Bulletin Series, Laboratory of Tree-Ring Research Bulletin No. 2*,
 590 XVI(4).
- 591 Scrucca, L. (2013). GA: A Package for Genetic Algorithms in R. *Journal of Statisti-*
 592 *cal Software*, 53(4), 1–37. DOI: 10.18637/jss.v053.i04
- 593 Stagge, J. H., Rosenberg, D. E., DeRose, R. J., & Rittenour, T. M. (2018). Monthly
 594 paleostreamflow reconstruction from annual tree-ring chronologies. *Journal of*
 595 *Hydrology*, 557, 791–804. DOI: 10.1016/j.jhydrol.2017.12.057
- 596 Stockton, C. W. (1971). *The Feasibility of Augmenting Hydrologic Records using*
 597 *Tree-Ring Data* (PhD Thesis). University of Arizona.
- 598 Stockton, C. W., & Jacoby, G. C. (1976). Long-term Surface-water Supply and
 599 Streamflow Trends in the Upper Colorado River Basin Based on Tree-ring
 600 Analyses. *Lake Powell Research Project Bulletin 18*.
- 601 Treydte, K. S., Schleser, G. H., Helle, G., Frank, D. C., Winiger, M., Haug, G. H., &
 602 Esper, J. (2006, apr). The twentieth century was the wettest period in north-
 603 ern Pakistan over the past millennium. *Nature*, 440(7088), 1179–1182. DOI:

- 604 10.1038/nature04743
- 605 Whitley, D. (1994, jun). A genetic algorithm tutorial. *Statistics and Computing*,
606 4(2). DOI: 10.1007/BF00175354
- 607 Woodhouse, C. A., Gray, S. T., & Meko, D. M. (2006). Updated streamflow re-
608 constructions for the Upper Colorado River Basin. *Water Resources Research*,
609 42(5), W05415. DOI: 10.1029/2005WR004455
- 610 Xu, C., Buckley, B. M., Promchote, P., Wang, S. S., Pumijumnong, N., An, W.,
611 ... Guo, Z. (2019). Increased Variability of Thailand’s Chao Phraya River
612 Peak Season Flow and Its Association With ENSO Variability: Evidence From
613 Tree Ring $\delta^{18}\text{O}$. *Geophysical Research Letters*, 46(9), 4863–4872. DOI:
614 10.1029/2018GL081458
- 615 Xu, C., Pumijumnong, N., Nakatsuka, T., Sano, M., & Guo, Z. (2018). Inter-annual
616 and multi-decadal variability of monsoon season rainfall in central Thailand
617 during the period 1804–1999, as inferred from tree ring oxygen isotopes. *Inter-
618 national Journal of Climatology*, 38(15), 5766–5776. DOI: 10.1002/joc.5859
- 619 Xu, C., Pumijumnong, N., Nakatsuka, T., Sano, M., & Li, Z. (2015). A tree-ring
620 cellulose $\delta^{18}\text{O}$ -based July–October precipitation reconstruction since AD
621 1828, northwest Thailand. *Journal of Hydrology*, 529(P2), 433–441. DOI:
622 10.1016/j.jhydrol.2015.02.037
- 623 Xu, C., Sano, M., & Nakatsuka, T. (2011, dec). Tree ring cellulose $\delta^{18}\text{O}$ of *Fok-
624 ienia hodginsii* in northern Laos: A promising proxy to reconstruct ENSO?
625 *Journal of Geophysical Research: Atmospheres*, 116(D24), D24109. DOI:
626 10.1029/2011JD016694
- 627 Xu, C., Sano, M., & Nakatsuka, T. (2013, sep). A 400-year record of hydrocli-
628 mate variability and local ENSO history in northern Southeast Asia inferred
629 from tree-ring $\delta^{18}\text{O}$. *Palaeogeography, Palaeoclimatology, Palaeoecology*, 386,
630 588–598. DOI: 10.1016/j.palaeo.2013.06.025
- 631 Xu, G., Liu, X., Trouet, V., Treydte, K., Wu, G., Chen, T., ... Qin, D. (2019, jan).
632 Regional drought shifts (1710–2010) in East Central Asia and linkages with
633 atmospheric circulation recorded in tree-ring $\delta^{18}\text{O}$. *Climate Dynamics*, 52,
634 713–727. DOI: 10.1007/s00382-018-4215-2
- 635 Zhu, M., Stott, L., Buckley, B. M., Yoshimura, K., & Ra, K. (2012, jun). Indo-
636 Pacific Warm Pool convection and ENSO since 1867 derived from Cambodian
637 pine tree cellulose oxygen isotopes. *Journal of Geophysical Research: Atmo-
638 spheres*, 117(D11), D11307. DOI: 10.1029/2011JD017198